Bone Reports 3 (2015) 40–47

Contents lists available at ScienceDirect

Bone Reports

journal homepage: www.elsevier.com/locate/bonr

# Copper accumulation in the sequestrum of medication-related osteonecrosis of the jaw

Tomoko Sugiyama [a], Motohiro Uo [b,c,*], Teruyasu Mizoguchi [c,d], Takahiro Wada [b], Daisuke Omagari [e], Kazuo Komiyama [e], Yoshiyuki Mori [a]

[a] Department of Dentistry, Oral and Maxillofacial Surgery, Jichi Medical University, 3311-1 Yakushiji, Shimotsuke, Tochigi 329-0498, Japan
[b] Advanced Biomaterials Department, Graduate School of Medical and Dental Sciences, Tokyo Medical and Dental University, 1-5-45 Yushima, Bunkyo-ku, Tokyo 113-8549, Japan
[c] Department of Materials Engineering, Graduate School of Engineering, The University of Tokyo, 7-3-1 Hongo, Bunkyo-ku, Tokyo 113-8656, Japan
[d] Department of Materials and Environmental Science, Institute of Industrial Science, The University of Tokyo, 4-6-1, Komaba, Meguro-ku, Tokyo 153-8505, Japan
[e] Department of Pathology, Nihon University School of Dentistry, 1-8-13 Kanda Surugadai, Chiyoda-ku, Tokyo 131-8310, Japan

ARTICLE INFO

*Article history:*
Received 18 April 2015
Received in revised form 30 July 2015
Accepted 5 August 2015
Available online 10 August 2015

*Keywords:*
Medication-related osteonecrosis of the jaw
Trace elements
Synchrotron radiation X-ray fluorescence analysis
Particle-induced X-ray emission analysis
X-ray absorption fine structure analysis

ABSTRACT

Bisphosphonates (BPs) have been widely, efficiently, and safely used for the treatment of various bone-related diseases such as osteoporosis. However, concerns about jaw osteonecrosis associated with oral treatment (medication-related osteonecrosis of the jaw [MRONJ]) have been increasing. Although many risk factors for MRONJ have been elucidated, its precise etiology and methods of prevention remain unknown. In this study, we have applied various elemental analysis methods for MRONJ specimens (e.g., X-ray fluorescence with synchrotron radiation [SR-XRF], particle-induced X-ray emission [PIXE], X-ray absorption fine structure [XAFS]) in order to reveal the accumulation and chemical state of trace bone minerals. In four MRONJ sequestra, the characteristic localization of copper (Cu) was observed by SR-XRF. Using micro-PIXE analysis, Cu looked to be localized near the edge of the trabecular bone. The chemical state of the accumulated Cu was estimated using XAFS and the possibility of a Cu–BP complex formation was assumed. Thus, in this study we argue for the feasibility of the trace element analysis to evaluate the potential pathophysiological mechanism of MRONJ.



## 1. Introduction

As synthetic analogues of pyrophosphate compounds, bisphosphonates (BPs) are selectively uptaken by osteoclasts and strongly inhibit bone resorption by inducing apoptosis (Iwata et al., 2006; Rodan and Fleisch, 1996; Viereck et al., 2002). BPs can be classified into two groups: non-nitrogen containing and nitrogen-containing. Nitrogen-containing BPs, a new-generation of BPs with different action mechanisms than non-nitrogen containing BPs, have been widely used for the treatment of osteoporosis, malignant hypercalcemia, solid cancers inducing bone metastasis, Paget's disease, and multiple myeloma (Russell et al., 2007; Yoneda et al., 2010). However, since Marx et al. in 2003 reported the first case of jaw osteonecrosis in a cancer patient received BPs following dental treatment (Marx, 2003), the reports of medication-related osteonecrosis of the jaw (MRONJ) have been increasing (Bamias et al., 2005). Although many factors related to MRONJ have been identified (Yoneda et al., 2010), such as BP formulation (Marx et al., 2007), local factors (e.g., tooth extraction and dental implants) (Ruggiero et al., 2004; Marx et al., 2005), systemic factors (e.g., anticancer drugs or steroids) (Khamaisi et al., 2007), genetic factors (e.g., presence of P450 CYP2C8) (Sarasquete et al., 2008), and other factors (e.g., drug use, smoking, alcohol) (Matthew and David, 2008; Wessel et al., 2008; Migliorati et al., 2006), the precise risk factors for developing MRONJ are unknown. Although guidelines and position papers suggest systemic management, patient education, antibacterial mouth rinse, oral hygiene maintenance, and BP withdrawal for patients classified as high-risk, there are no clear evidence-based medicine for MRONJ treatment (Yoneda et al., 2010; Ruggiero et al., 2009). Therefore, the establishment of diagnostic markers for MRONJ risk assessment and prevention is urgently needed.

Experimental studies to reveal changes in the chemical components of bone exhibiting MRONJ development have been carried out for serum biomarkers and bone minerals. The relationship between serum biomarkers (e.g., parathyroid hormone (Kim et al., 2013) or C-terminal telopeptide of collagen I (Marx et al., 2007)) and MRONJ development has been studied, although a clear linkage has not been found. Concerning bone minerals, Lowe et al. reported that plasma zinc (Zn) concentration in osteoporosis patients was significantly lower than that in healthy persons, while no significant changes were observed in plasma copper (Cu) concentration (Lowe et al., 2002). Koçer et al.

* Corresponding author at: Advanced Biomaterials Department, Graduate School of Medical and Dental Sciences, Tokyo Medical and Dental University, Japan.
*E-mail address:* uo.abm@tmd.ac.jp (M. Uo).

http://dx.doi.org/10.1016/j.bonr.2015.08.001

reported that BP treatment decreases Zn and Cu in the oral epithelium of rats (Koçer et al., 2013). Therefore, Zn and Cu analysis may be the possible indices to reveal the MRONJ pathophysiological mechanism. However, no literature presents a compelling argument for how to evaluate Zn and Cu levels in MRONJ patients. In addition, those studies discussed the average concentration of Zn and Cu in serum, plasma, and entire tissue. However, those elements would not be homogeneously distributed in bone. Concerning Zn, Gomez et al. demonstrated that it can be detected at the osteon surface and the calcification front (Gomez et al., 1999). Therefore, the quantitative and distribution analyses of Zn and Cu in sequestrum of MRONJ patients might provide useful information to reveal pathophysiology or further risk assessment. However, the concentration of these elements in bone is quite low, so a highly sensitive and position-specific elemental analysis method is required for this purpose. The authors have applied the detection and chemical state analysis methods of metallic trace elements to analyze soft tissues (Sugiyama et al., 2014, 2015; Uo et al., 2015). Synchrotron radiation-induced X-ray fluorescence spectroscopy (SR-XRF) provides information on elements in specimens and X-ray absorption fine structure (XAFS) analysis provides information on the chemical state of target elements. Using these methods, trace metallic elements in biopsy specimens can be detected and analyzed.

In this study, hence, we focus on the distribution and chemical state of trace essential elements contained in bone. SR-XRF and micro-focused particle-induced X-ray emission spectroscopy (micro-PIXE) were applied to an elemental distribution analysis of thin-sectioned specimens of MRONJ sequestrum. The chemical state for concentrated elements in bone was also estimated with an XAFS analysis of the concentrated regions. Subsequently, we estimated the localization of trace mineral accumulation and distribution, and their chemical state in the MRONJ sequestrum.

## 2. Materials and methods

### 2.1. Bone specimens

Bone specimens were supplied by Jichi Medical University Hospital, Tochigi, Japan. The samples included four MRONJ-induced sequestrum specimens that were exposed to BP therapy (alendronate [ALN] and zoledronate [ZOL]) and two torus mandibularis specimens that were not exposed to BP therapy. Torus mandibularis is non-neoplastic hyperplasia disease. Histopathologically, laminar bone cortex structure without dysplasia is observed. Therefore, we used torus mandibularis as the control (CON). All patients provided informed consent and the study protocol was approved by the Ethical Committee of Jichi Medical University Hospital (A14-181). Table 1 shows the clinical data for all specimens.

Specimen #1 included mandibular bone tissue from a patient who had received alendronate for osteoporosis. She had been treated with a bridge-type prosthesis eight years earlier, and received BP therapy beginning five years earlier. Direct contact between the two dummy teeth and gingiva and bone exposure in the same region were observed. This patient was diagnosed with MRONJ in light of clinical findings, histopathological findings, and her medical background of receiving BPs.

Specimen #3 included mandibular bone tissue from a patient who had received ZOL for bone metastasis of mammary carcinoma. After her right mandibular molar was extracted, she received BP therapy for a period of two years. Since that time, she experienced strong pain, pus discharge, and bone exposure. This patient was diagnosed with MRONJ using clinical findings, histopathological findings, and medical background.

Specimen #5 included mandibular bone tissue from a patient who had no systemic complications and had not received BPs. He presented to our office with a complaint after bone resection, wherein there was bone prominence in the mandibular lingual region. The denture had pressured onto this area, and the pain and a decubital ulcer were observed. The patient was diagnosed with torus mandibularis using clinical and histopathological findings. The clinical history of the remaining specimens (#2, #4, and #6) is described in "Supplementary material."

All bone specimens were fixed in 4% phosphate-buffered saline–formalin. Decalcification was performed in ethylenediaminetetraacetic acid (EDTA) for three to five days. The specimens were embedded in paraffin and sliced into two thicknesses (4 μm and 8 μm). The 4-μm sample, which was stained with hematoxylin and eosin (H&E), was placed adjacent to the 8-μm sample on Kapton film (12.5 μm thick; Du Pont-Toray Co., Ltd., Tokyo, Japan) and subjected to the following elemental analyses.

### 2.2. Elemental distribution analysis

#### 2.2.1. Synchrotron radiation X-ray fluorescence spectroscopy (SR-XRF) analysis

XRF analyses of the six specimens were carried out at BL-4A of the Photon Factory at the High Energy Accelerator Research Organization in Tsukuba, Japan. The incident X-ray (12.9 keV) was focused to a 30-μm region using polycapillary optics, and the specimen was irradiated. The specimen stage was scanned in the X–Y plane, two dimensionally, to obtain elemental distribution images. The scanning areas varied within several millimeters, and the scanning steps varied from 40 μm to 100 μm. The obtained XRF data were processed with PyMCA software (Version 4.7.3) after elemental distribution images were obtained.

#### 2.2.2. Preparation of the thin film standard for quantitative analysis

Thin film standard specimens of zinc (Zn) and copper (Cu) were prepared using organometallic compounds and methacrylate resins. First, we prepared the resin monomer matrix: bisphenol A-glycidyl methacrylate (Shin-Nakamura Chemical, Wakayama, Japan) and triethylene glycol dimethacrylate (Tokyo Chemical Industry, Tokyo, Japan) were mixed to a 1:2 weight ratio to be a base monomer. Benzoyl peroxide (Tokyo Chemical Industry, Tokyo, Japan) and camphorquinone (Sigma Aldrich, St. Louis, MO, USA) were added as a polymerization initiator. The acetylacetonates with Zn and Cu (Dojindo, Kumamoto, Japan) were dissolved into the monomer at 0 to 40 ppm. The prepared monomer was spread over the glass plate and polymerized with photo-curing and

**Table 1**
Clinical data for the patients.

| No. | Sex | Age | Diagnosis | BPs | Stage at initial visit | BPs receiving period | Primary disease | Corticosteroid | Site | Trigger dental treatment and oral condition |
|---|---|---|---|---|---|---|---|---|---|---|
| #1 | F | 72 | MRONJ | ALN p.o. | 2 | 5 years | Osteoporosis | – | Mandibula | Pressure onto the gingiva from two dummy teeth of bridge-type prostheses |
| #2 | F | 51 | MRONJ | ALN p.o. | 2 | 6 years | Osteoporosis | PSL 5 mg | Mandibula | Tooth extraction |
| #3 | F | 65 | MRONJ | ZOL i.v. | 2 | 2 years | Bone metastasis of mammary carcinoma | – | Mandibula | Tooth extraction |
| #4 | M | 74 | MRONJ | ZOL i.v. | 2 | 2 years | Bone metastasis of prostatic carcinoma | – | Maxilla | Chronic apical periodontitis |
| #5 | M | 64 | Torus mandibularis | – | – | – | – | – | Mandibula | – |
| #6 | F | 48 | Torus mandibularis | – | – | – | – | – | Mandibula | – |

MRONJ—medication-related osteonecrosis of the jaw; F—female; M—male; ALN—alendronate; ZOL—zoledronate; PSL—prednisolone; p.o.— per os; i.v.—intravenous.

heat-curing. The thickness of the prepared thin film standards was measured in micrometers. The XRF analyses of the standards were carried out with the same conditions as described above. The co-relation between the fluorescence X-ray intensity and the element concentration were obtained from the calibration curves.

*2.2.3. Micro-focused particle induced X-ray emission spectroscopy (Micro-PIXE) analysis*

In order to visualize the high-resolution elemental distribution images, micro-PIXE analysis was carried out at the National Institute of Radiological Sciences (Chiba, Japan). An accelerated and micro-focused proton beam (3.0 MeV, 2-μm beam diameter) with raster scanning was applied over the target area of the specimen (500 × 500 μm). The generated characteristic X-rays were collected using Si(Li) and CdTe detectors to obtain the elemental distribution images and the characteristic X-ray spectra. The obtained data were processed with OMDAQ2007 software (Version 1.3.71.669), and the elemental distribution images and characteristic X-ray spectra of the region of interest were collected.

*2.3. X-ray absorption fine structure (XAFS) analysis*

The X-ray absorption spectrum around the specific energy of the target elements called the "absorption edge" reflects the surrounding structure and the chemical state of the element. The specific structure on the spectrum is known as XAFS. Comparison of the XAFS spectrum with those of reference materials can reveal the chemical state of the target elements. For the typically accumulated metallic elements, XAFS analyses were carried out to determine the chemical states of the elements. XAFS analyses were also conducted at BL-4A of the Photon Factory. XAFS spectra of accumulated Cu in sequestrum specimens were measured with the fluorescent XAFS method. For comparison, Cu metal and copper (I) oxide ($Cu_2O$) were also measured as reference specimens.

*2.4. Computational procedure of XAFS spectra*

Cu-incorporated hydroxyapatite (Cu–HAp) and Cu-alendronate complex (Cu–ALN) were not available as reference materials for XAFS measurements. Therefore, theoretical Cu K-edge XAFS spectra for those materials were simulated using the first principles plane wave basis pseudopotential method (CASTEP code) (Clark et al., 2005; Gao et al., 2008). Generalized gradient approximation (GGA) was used as an exchange–correlation interaction, and the plane wave cutoff energy was set to 400 eV. Spin-polarization was considered in the calculations, and on-site Coulomb interaction (U = 6.5 eV) was used for Cu-d orbital. To account for a core hole effect, a special ultrasoft pseudo-potential designed for excited atoms with a core hole was employed in the excited Cu atom. Theoretical transition energy was estimated by the same method as described in a previous report (Mizoguchi et al., 2009). This method can quantitatively reproduce the amount of chemical shift (Mizoguchi et al., 2009). The detailed conditions for calculations followed the procedures outlined in a previous report (Matsunaga et al., 2010). The crystal structure of Cu–HAp and Cu–ALN was optimized until the residual force lowered to 0.03 eV/Å, as described in previous reports (Matsunaga et al., 2010; Demoro et al., 2012).

## 3. Results

*3.1. Histopathological analysis*

Fig. 1 shows the H&E stained images of the specimens #1 (ALN), #3 (ZOL), and #5 (CON). All specimens had characteristic features of necrotic bone: osteomyelitis containing necrotic bone with no osteoblasts, no osteoclasts, and granulation tissue with inflammatory cell infiltration. Moreover, in specimens #1 and #3, fibrosis of the medullary space and *Actinomyces* colonies were observed. (The H&E stained images of specimens #2 [ALN], #4 [ZOL], and #6 [CON] are shown in Fig. S1 of the "Supplementary material.").

*3.2. Elemental distribution analysis*

Fig. 2 shows the elemental distribution (phosphorus [P], calcium [Ca], Cu, and Zn) images of entire specimens #1 (ALN), #3 (ZOL), and #5 (CON) obtained using SR-XRF with 100 μm step. The observation regions in each were the same as the regions shown in Fig. 1A. The P distribution images show the entire shape of the specimens and the similarity of the observational regions could be confirmed by the shape similarity with the H&E stained images shown in Fig. 1. Ca distribution images of all figures show no characteristic localization and complete demineralization could be observed. In contrast, the Cu distribution images show significant differences between MRONJ sequestrum (#1 and #3) and control (#5). Characteristic accumulation (line-shaped, not diffusible) of Cu was observed in the MRONJ sequestrum, hence no accumulation was observed in the control. Zn showed a similar tendency. In order to visualize more detailed distribution of Cu and Zn in specimens #1 and #3, the white box regions of Fig. 2 were analyzed using SR-XRF with a higher resolution (40 μm step), as shown in Fig. 3. MRONJ sequestrum showed characteristic distribution of Cu and Zn; these elements were clearly localized around the bone trabecula structure.

The fluorescence X-ray (XRF) spectra of Cu-localized spots shown in Fig. 2 are compiled in Fig. 4 in order to compare the intensity of the fluorescence X-ray of the detected elements. In order to compare the accumulated elements between the regions with characteristic elemental accumulation, XRF spectra at the spots (indicated with white arrows in Fig. 2) are shown in Fig. 4. Significantly strong peaks of Cu were observed in MRONJ specimens (#1 and #3). Very small peaks of Ca indicated successful demineralization of all specimens. (The corresponding data for Figs. 2 to 4 of specimens #2, #4, and #6 are shown in Figs. S2 to S4 of the "Supplementary material".)

Fig. 5 shows high-resolution Cu distribution images of specimens #1 and #3 obtained by micro-PIXE of the white rectangular region in Fig. 3. The H&E stained images of the corresponding region are also shown. Sulfur (S) was contained in the organic components of the sequestrum, thus the entire shape of the observation region could be identified and coincided well with the H&E image. Cu showed obvious localization along the edge of the bone trabecula.

Fig. 6 shows the calibration curve for the Cu standard specimens. Good linearity was obtained for the relationship between the element concentration and the fluorescence X-ray intensity, which were normalized with the specimen thickness for both elements. The raw intensity and thickness (8 μm) normalized intensity of the fluorescence X-ray of Cu at spots (#1, #3, and #5 in Fig. 2, and #2, #4, and #6 in Fig. S2 in the "Supplementary material") are shown in Table 2. Using this relation for the above intensities of Cu at the localized spots could also be estimated, as shown in Table 2. The extremely high concentration of Cu at the accumulated spots in specimens #1 to #4, which were derived from the MRONJ specimens, could be identified compared to the bone that were not exposed to BPs (specimens #5 and #6). Therefore, an abnormally high level of Cu accumulation in MRONJ sequestra was revealed.

*3.3. XAFS analysis and the simulation*

Fig. 7 shows the XAFS spectra of Cu at spots #1 and #3 of specimens #1 and #3, and also that of the reference materials (Cu metal and $Cu_2O$). The XAFS spectra suggested that Cu in spot #1 and spot #3 was in a similar chemical state, but this state differed from that of the reference materials (e.g., Cu metal and oxide). Therefore, the accumulated Cu in MRONJ sequestra was not in those states. The calculated XAFS spectra of Cu metal, Cu–ALN, and Cu–HAp is also shown in Fig. 7. It was

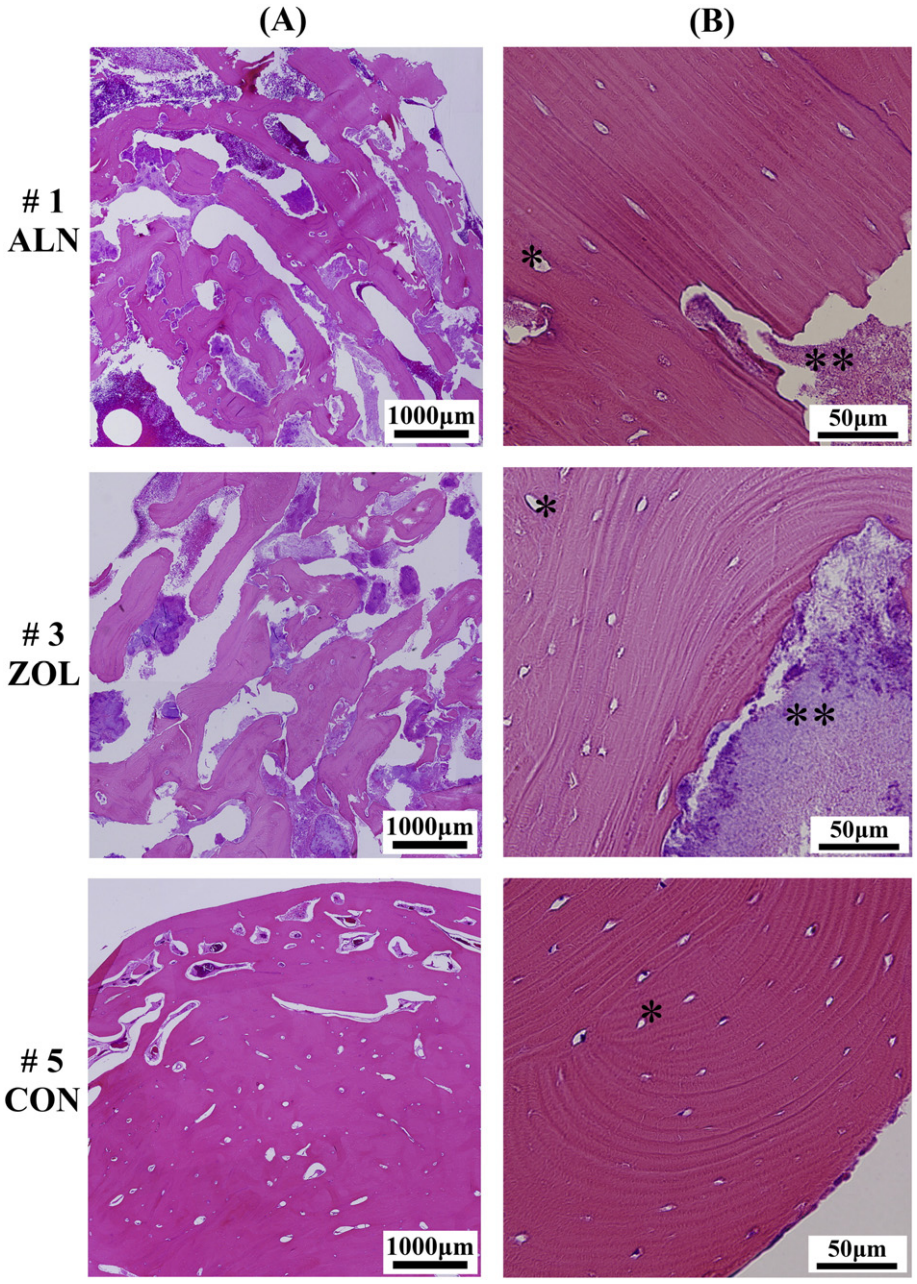


**Fig. 1.** Histopathological images (hematoxylin and eosin (H&E) staining) of specimen #1 exposed to alendronate (ALN), specimen #3 exposed to zoledronate (ZOL), and the control specimen #5 not exposed to BPs (CON). (A) low magnification and (B) high magnification. All sequestrum specimens had the characteristics of necrotic bone: no osteoblasts in the bone cavity (*), no osteoclasts at the edge of bone trabecula, and granulation tissue with inflammatory cells. Moreover, in specimens #1 and #3, fibrosis of medullary space and *Actinomyces* colony (**) were observed.

impossible to reproduce the measured XAFS spectrum with a computer simulation because the measurements were affected by various factors (e.g., fractuations and defects of the structure of target substance and also fractuations of measurement facilities). Therefore, measured and simulated spectra were not completely matched, even for Cu metal that had a simple crystal structure. Therefore, the validity of simulation can be estimated by the absorption edge energy and the outline of the spectrum around the edge. To show the outline of the calculated spectra, smoothened spectra are shown in Fig. 7. (The original spectra are shown in Fig. S5 of the "Supplementary material".) The outline of the measured Cu metal spectrum around the absorption edge (8975–8990 eV), which showed a gradual increase, was well reproduced in the simulation, thus those simulated spectra were valid. In comparison with the spectra of spots #1 and #3 to the simulated spectra of Cu–ALN and Cu–HAp, the absorption edge energy of spots #1 and #3 ($E_{measured}$) was closer to that of the simulated Cu–ALN ($E_{Cu-ALN}$) than that of the Cu–HAp ($E_{Cu-HAp}$). In addition, a gradual increase of the measured absorption spectra in spots #1 and #3 around the absorption edge (8980–8990 eV) was similar to that of Cu–ALN.

## 4. Discussion

Bisphosphonates have a high affinity for bone minerals (Rogers et al., 1997; Russell et al., 2007). They comprise two phosphonate groups attached to a single carbon atom, the molecular framework of a P–C–P structure, which can chelate calcium ions through the phosphonate groups. BPs are incorporated into osteoclasts during bone remodeling, and bone resorption is inhibited by inducing apoptosis of osteoclasts (Rogers et al., 2000; Russell et al., 2007). Therefore, BPs are a very effective treatment for various bone diseases.

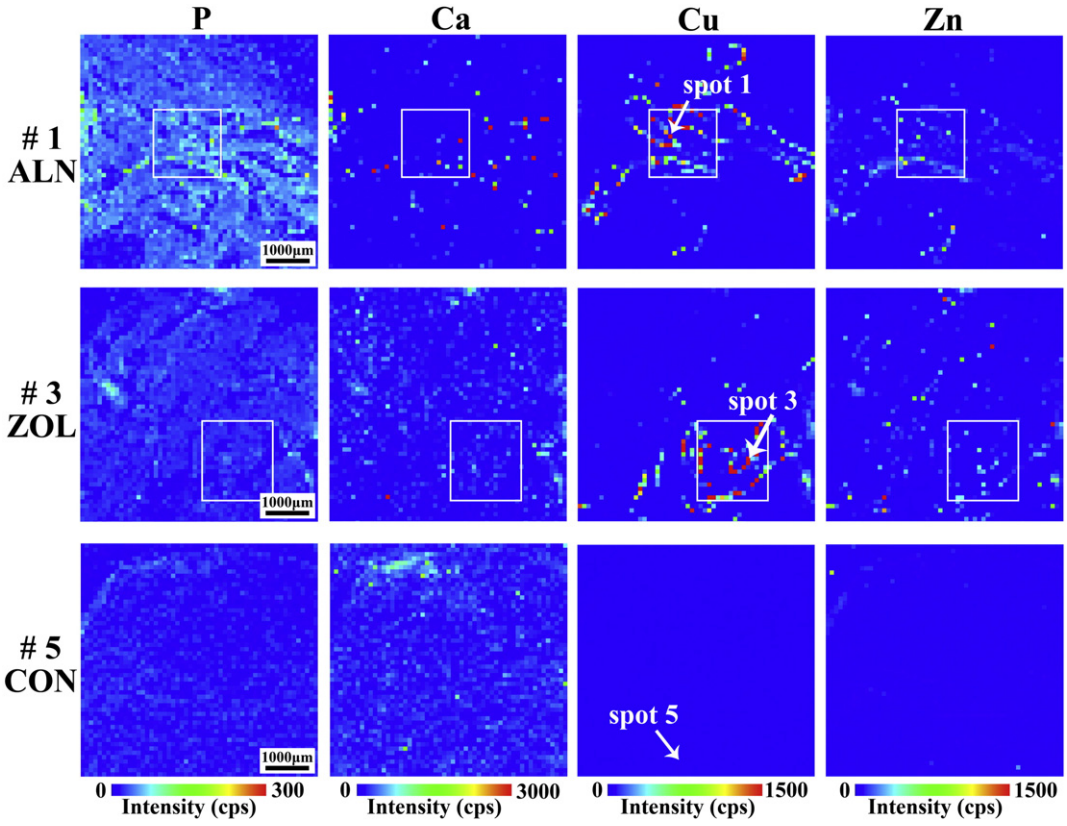


**Fig. 2.** Elemental distribution images of specimens #1, #3, and #5 obtained by SR-XRF. The observation areas were the same as those for Fig. 1(A) in each specimen. Clear Cu and Zn accumulation may be observed over the entire area of the MRONJ sequestra (#1 and #3). In contrast, accumulation could not be identified in the control specimen (#5). P and Ca could not be clearly detected in all specimens.

However, we have been faced with a serious problem that calls for an effective mechanism to identify the biomarkers or indices of MRONJ. Nitrogen analysis has also been used to estimate BP accumulation in bone (Schaudinn et al., 2012), but an effective single factor has not been identified.

In this study, we revealed a peculiar change of bone minerals, especially Cu, in the MRONJ sequestrum. Specimens #5 and #6, which were not exposed to BP therapy, showed no characteristic accumulation of Cu (Figs. 2 and S2). In contrast, specimens #1 to #4 (MRONJ sequestra) showed clear and line-shaped accumulation of Cu (Figs. 2,

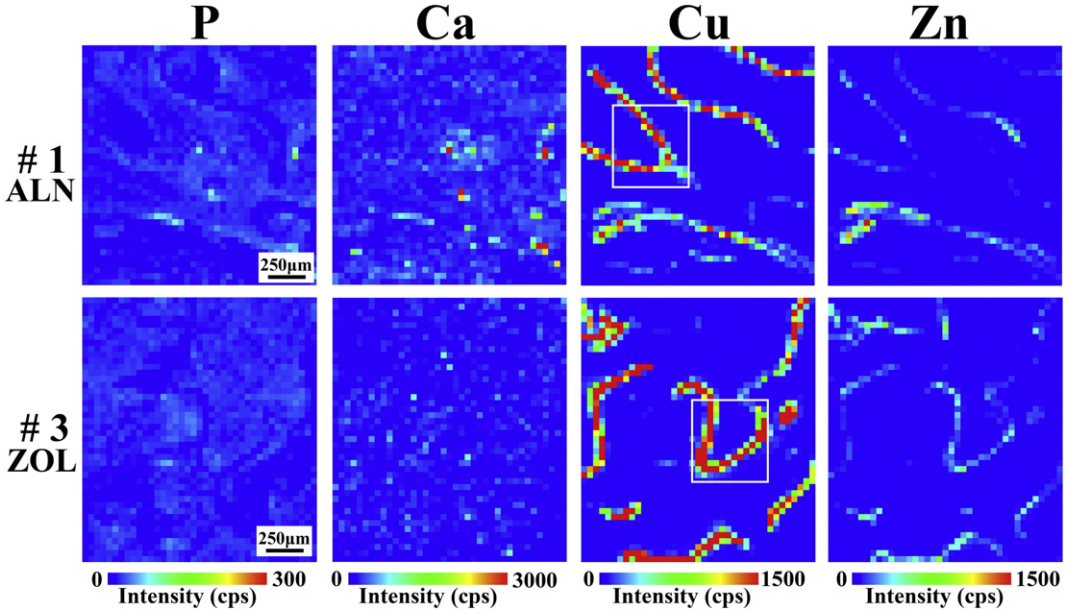


**Fig. 3.** The detailed elemental distribution images of the white rectangular region of Fig. 2 for specimens #1 and #3 obtained by SR-XRF. Significant Cu and Zn accumulation were observed in the MRONJ sequestra. Moreover, the accumulation of these elements was similarly line-shaped.

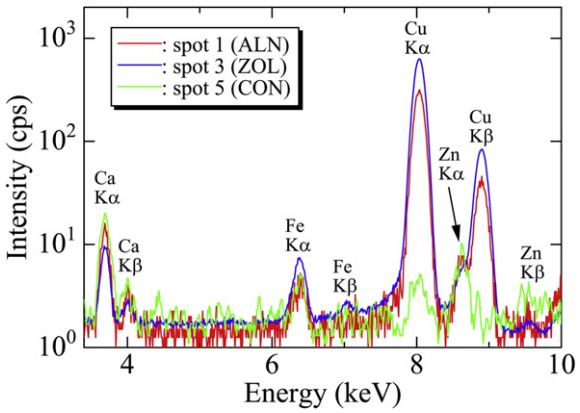


**Fig. 4.** XRF spectrum at the accumulated spots (#1 to #3) of Cu is indicated with *arrows* in Fig. 2. Spot #1 (ALN) and spot #3 (ZOL) showed clear fluorescence X-ray peaks for Cu, whereas those of Ca and Fe were weak. Spot #5 (CON) showed a weak elemental peak.

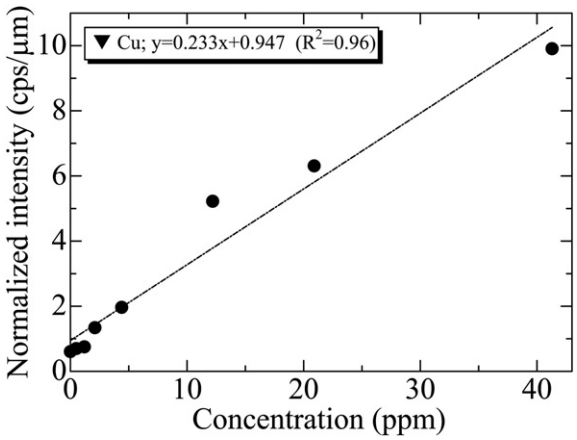


**Fig. 6.** Calibration curves of the prepared thin film standard specimens for Cu. A good linear relationship between the elemental concentration and thickness-normalized fluorescence X-ray intensity was obtained.

3, S2, and S3). Detailed distribution in Fig. 5 shows Cu localization along the edge of the bone trabecula. At Cu localization spots, XRF spectra (Figs. 6 and S4) show extremely strong peaks assigned to Cu compared to that of Ca. The low intensity of Ca peaks suggests the complete demineralization treatment of all bone specimens. Hence, Cu was clearly retained and localized. As shown in Table 2, the concentrations of Cu in the MRONJ sequestra specimens (#1 to #4) were estimated to be between 600 to 5000 ppm. In contrast, Cu concentrations in the control specimens (#5 and #6) were estimated at around 20 to 100 ppm. The concentrations of Cu in the MRONJ specimens were more than two orders higher than that in the normal bone. The Cu concentration of normal bone tissue has been reported as 0.77 ± 0.28 (ppm) for Cu (Basle et al., 1990). The estimated Cu concentrations in MRONJ sequestra were more than three orders higher than the reported average Cu concentration in normal bone. In those specimens, demineralization could be completed because Ca and P were slightly detected for entire specimens in elemental distribution images (Figs. 2, 3, S2, and S3) and also in XRF spectra (Figs. 4 and S4). In normal bone, Cu is incorporated in the HAp-substituting Ca site. This is one possible candidate where Cu may accumulate. However, if Cu is incorporated in HAp of MRONJ sequestrum, it could be demineralized with EDTA solution. Therefore, we suggest that Cu may form and retain a stable complex that cannot be removed by the demineralization process.

Considering the form of accumulated Cu, it is important to note that Cu accumulated near the edge of bone trabecular (Fig. 5). In the vicinity of bone trabecula, osteoclasts exist in a high population for bone resorption and bone is vigorously remodeled. It is well known that BPs incorporated into osteoclasts inhibit bone resorption. Therefore, BP concentrations in Cu-accumulated regions would be high (for the osteoclast population) and there would be a generally high concentration of BPs. Therefore, Cu–BP complex could be suggested as a possible candidate substance for the accumulated form of Cu.

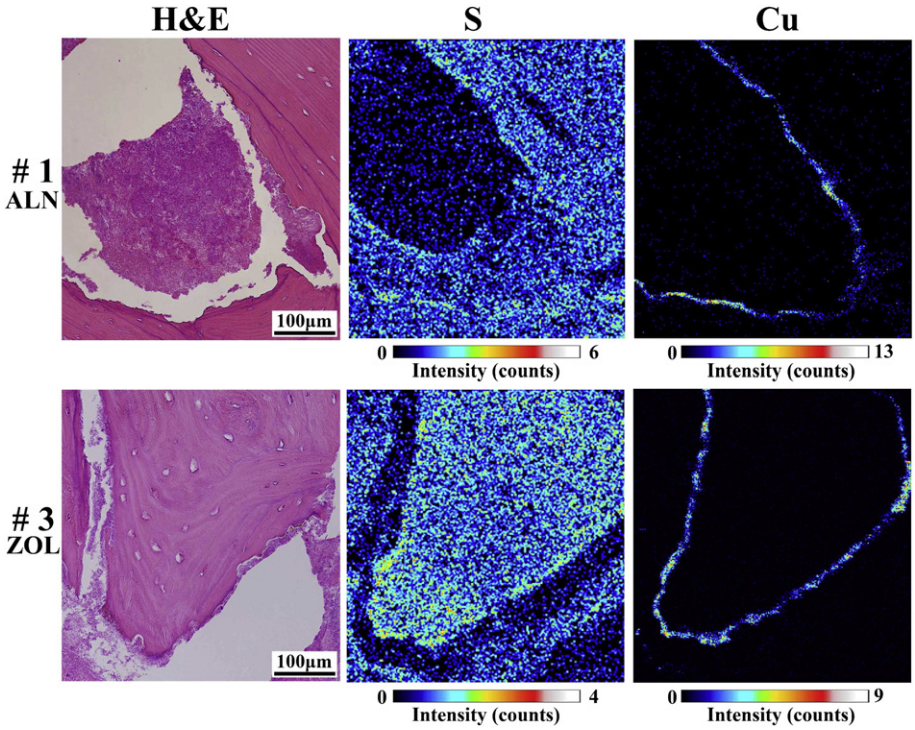


**Fig. 5.** High-resolution elemental distribution images for specimens #1 and #3 obtained by micro-PIXE and H&E stain of the corresponding region. The shape of the entire specimen can be identified by S distribution. Cu looked to be localized among the near edge of the bone trabecula.

**Table 2**
Fluorescence X-ray intensities of Cu at spot #1 to spot #6 and the estimated concentration using thin film standard specimens.

| Spot | BPs | Fluorescence X-ray intensity (cps) | Intensity normalized with thickness (8 μm) | Estimated concentration (ppm) |
|---|---|---|---|---|
| #1 | ALN | 5474 | 684 | 2900 |
| #2 | | 1102 | 138 | 590 |
| #3 | ZOL | 9372 | 1170 | 5000 |
| #4 | | 5915 | 739 | 3200 |
| #5 | CON | 47 | 6 | 22 |
| #6 | | 190 | 24 | 99 |

Various metal BP complexes have been studied for industrial use because of their electrical and optical properties (Katz et al., 1991; Snover et al., 1996; Neff et al., 1999) as well as the pharmacological effects (Demoro et al., 2012; Wolf and Stoller, 1994). The purified substances of Cu–incorporated HAp (Cu–HAp) and Cu–BP complex were not available for testing. Therefore, we simulated the XAFS spectra of the two substances [Cu–HAp and Cu–alendronate complex (Cu–ALN)] and compared the measured XAFS spectra from specimen #1 and specimen #3 (Fig. 7). Because of the limitation of theoretical simulation, the complete consistency of the measured spectra of specimen #1 and specimen #3 and the simulated spectra depicted in Fig. 7 could not be achieved. Features of the XAFS spectra at spots #1 and #3 include a higher absorption edge energy ($E_{measured}$) and a gradual increase of the absorption around the edge (8980–8990 eV). Measured spectra of Cu metal and $Cu_2O$, and simulated spectra of Cu–HAp could not reproduce the aforementioned features. The simulated spectrum of Cu–ALN can only reproduce the aforementioned features among the measured and simulated materials. In consideration of the accumulated location of Cu (near the edge of bone trabecula) and the similarity in XAFS spectra, it may be assumed that Cu accumulated and localized in the MRONJ sequestrum as Cu–BP complex, e.g., Cu–ALN.

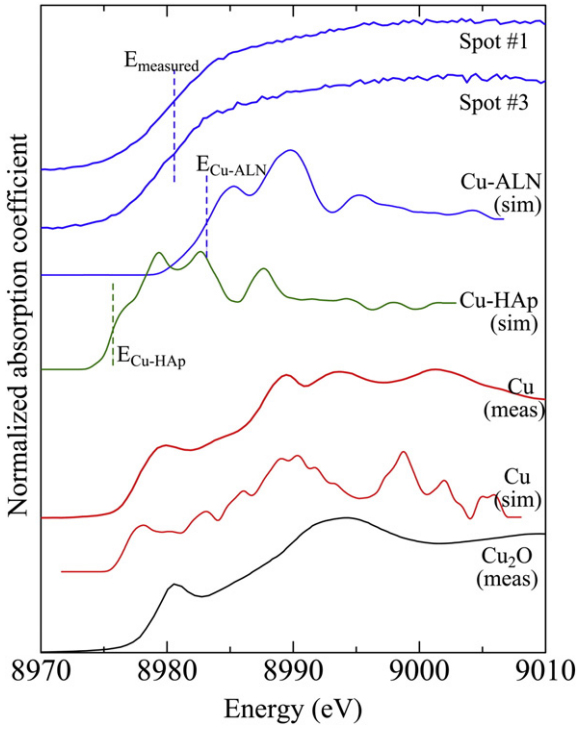


**Fig. 7.** The measured spectra (meas) of the MRONJ sequestra and the reference materials (Cu metal and $Cu_2O$) and simulated spectra (sim) of the Cu-alendronate complex (Cu–ALN), Cu–incorporated HAp (Cu–HAp), and Cu metal. The measured spectra of the MRONJ sequestra were different from Cu metal and $Cu_2O$. Absorption edge energy of measured spectra, simulated spectra of Cu–ALN and Cu–HAp are indicated as $E_{measured}$, $E_{Cu-ALN}$, and $E_{Cu-HAp}$, respectively. The absorption edge energy and the shape of spectra of the measured spectra at spots #1 and #3 were similar to those of the simulated spectrum of Cu–ALN when compared with other materials.

In this study, we analyzed only four MRONJ sequestra and two control bone specimens without BP administration. Because of the small specimen size, it is difficult to conclusively state the effects of Cu accumulation and its relationship with MRONJ pathogenesis. However, the characteristic accumulation of Cu in MRONJ sequestra in a high concentration, even after demineralization, could not be explained as incorporation into HAp. In addition, with the localization of Cu along the edge of the bone trabecula and the similarity of XAFS spectra of Cu in the MRONJ sequestra and Cu–ALN, the possibility of a relationship between Cu and BP accumulation could be suggested.

The present study was a preliminary trial to estimate the feasibility of trace metallic element analysis for the study of MRONJ pathogenesis. Therefore, a future study is necessary to confirm the aforementioned assumption concerning the Cu and BP relationship and its effect on MRONJ:

1) Cu accumulation and distribution should be estimated for MRONJ sequestra and for other bone diseases with and without BPs.
2) BP distribution in MRONJ and control bone specimens and the relation to Cu distribution should be estimated; and the chemical state of Cu accumulated in MRONJ using the XAFS measurement compared with other various Cu compounds and synthesized Cu–HAp, Cu–ALN and other Cu–BPs complexes should be confirmed.

Future studies concerning trace metallic element accumulation and localization in MRONJ sequestrum and their relation to Cu content in blood, urine, and other tissues might be useful indices to reveal the pathophysiological mechanism of MRONJ. In clinical application, a position paper from the American Association of Oral and Maxillofacial Surgery (Ruggiero et al., 2009) suggests “development of valid MRONJ risk assessment tools” for future study. The abnormal accumulation of Cu in bone might be a possible candidate index for MRONJ risk assessment.

## 5. Conclusion

In this study, we successfully detected the characteristic accumulation of Cu in MRONJ samples by using SR-XRF and micro-PIXE, and the chemical state of Cu was estimated using XAFS. The estimated concentration of accumulated Cu in the MRONJ sequestrum was much higher than that in normal bone, even after demineralization. From the distribution and chemical state of the accumulated Cu, the possibility of accumulation as a Cu–BP complex was assumed. Hence, the trace elemental analysis may provide useful indices to reveal the pathophysiological mechanism of MRONJ.

## Acknowledgments

The SR-XRF and XAFS measurements were performed with approval of the Photon Factory Program Advisory Committee (Proposal No. 2014G017). This work was financially supported by the Japan Society for the Promotion of Science (JSPS) KAKENHI (15K15721, 25106003, and 26249092). T. Sugiyama was supported by a research fellowship for young scientists from the JSPS. The authors would also like to thank Prof. N. Fukushima and Prof. T. Niki of the Department of Diagnostic Pathology, Jichi Medical University, for assisting with the sample preparation.

## Appendix A. Supplementary data

Supplementary data to this article can be found online at http://dx.doi.org/10.1016/j.bonr.2015.08.001.

## References


Bamias, A., Kastritis, E., Bamia, C., Moulopoulos, L.A., Melakopoulos, I., Bozas, G., Koutsoukou, V., Gika, D., Anagnostopoulos, A., Papadimitriou, C., Terpos, E., Dimopoulos, M.A., 2005. Osteonecrosis of the jaw in cancer after treatment with bisphosphonates: Incidence and risk factors. J. Clin. Oncol. 23, 8580–8587.

Basle, M.F., Mauras, Y., Audran, M., Clochon, P., Rebel, A., Allain, P., 1990. Concentration of bone elements in osteoporosis. J. Bone Mineral. Res. 5, 41–47.

Clark, S.J., Segall, M.D., Pickard, C.J., Hasnip, P.J., Probert, M.J., Refso, K., Payne, M.C., 2005. First principles methods using CASTEP. Z. Kristallogr. 220, 567–570.

Demoro, B., Caruso, F., Rossi, M., Benítez, D., González, M., Cerecetto, H., Galizzi, M., Malayil, L., Docampo, R., Faccio, R., Mombrú, Á.W., Gambino, D., Otero, L., 2012. Bisphosphonate metal complexes as selective inhibitors of *Trypanosoma cruzi* farnesyl diphosphate synthase. Dalton Trans. 41, 6468–6476.

Gao, S.P., Pickard, C.J., Payne, M.C., Zhu, J., Yuan, J., 2008. Theory of core-hole effects in 1s core-level spectroscopy of the first-row elements. Phys. Rev. B 77 115122.

Gomez, S., Rizzo, R., Pozzi-Mucelli, M., Bonucci, E., Vittur, F., 1999. Zinc mapping in bone tissues by histochemistry and synchrotron radiation-induced x-ray emission: Correlation with the distribution of alkaline phosphatase. Bone 25, 33–38.

Iwata, K., Li, J., Follet, H., Phipps, R.J., Burr, D.B., 2006. Bisphosphonates suppress periosteal osteoblast activity independently of resorption in rat femur and tibia. Bone 39, 1053–1058.

Katz, H.E., Scheller, G., Putvinski, T.M., Schilling, M.L., Wilson, W.L., Chidsey, C.E.D., 1991. Polar orientation of dyes in robust multilayers by zirconium phosphate–phosphonate interlayers. Science 254, 1485–1487.

Khamaisi, M., Regev, E., Yarom, N., Avni, B., Leitersdorf, E., Raz, I., Elad, S., 2007. Possible association between diabetes and bisphosphonate-related jaw osteonecrosis. J. Clin. Endocrinol. Metab. 92, 1172–1175.

Kim, J.W., Kong, K.A., Kim, S.J., Choi, S.K., Cha, I.H., Kim, M.R., 2013. Prospective biomarker evaluation in patients with osteonecrosis of the jaw who received bisphosphonates. Bone 57, 201–205.

Koçer, G., Nazıroğlu, M., Çelik, Ö., Önal, L., Özçelik, D., Koçer, M., Sönmez, T.T., 2013. Basic fibroblast growth factor attenuates bisphosphonate-induced oxidative injury but decreases zinc and copper levels in oral epithelium of rat. Biol. Trace Elem. Res. 153, 251–256.

Lowe, N.M., Fraser, W.D., Jackson, M.J., 2002. Is there a potential therapeutic value of copper and zinc for osteoporosis? Proc. Nutr. Soc. 61, 181–185.

Marx, R.E., 2003. Pamidronate (Aredia) and zoledronate (Zometa) induced avascular necrosis of the jaw: A growing epidemic. J. Oral Maxillofac. Surg. 61, 1115–1118.

Marx, R.E., Sawatari, Y., Fortin, M., Broumand, V., 2005. Bisphosphonate-induced exposed bone (osteonecrosis/osteopetrosis) of the jaws: Risk factors, recognition, prevention, and treatment. J. Oral Maxillofac. Surg. 63, 1567–1575.

Marx, R.E., Cillo Jr., J.E., Ulloa, J.J., 2007. Oral bisphosphonate-induced osteonecrosis: Risk factors, prediction of risk using serum CTX testing, prevention, and treatment. J. Oral Maxillofac. Surg. 65, 2397–2410.

Matsunaga, K., Murata, H., Mizoguchi, T., Nakahira, A., 2010. Mechanism of incorporation of zinc into hydroxyapatite. Acta Biomater. 6, 2289–2293.

Matthew, R.A., David, B.B., 2008. Mandible matrix necrosis in Beagle dogs after 3 years of daily oral bisphosphonate treatment. J. Oral Maxillofac. Surg. 66, 987–994.

Migliorati, C.A., Siegel, M.A., Elting, L.S., 2006. Bisphosphonate-associated osteonecrosis: A long-term complication of bisphosphonate treatment. Lancet Oncol. 7, 508–514.

Mizoguchi, T., Tanaka, I., Gao, S., Pickard, C.J., 2009. First principles calculation of spectral feature, chemical shift, and absolute threshold of ELNES and XANES using plane wave pseudopotential method. J. Phys. Condens. Matter 21, 104204-1–104204-6.

Neff, G.A., Helfrich, M.R., Page, C.J., 1999. Metal-bisphosphonate multilayer thin films with nonlinear optical activity. Phosphorus Sulfur Silicon Relat. Elem. 144, 53–56.

Rodan, G.A., Fleisch, H.A., 1996. Bisphosphonates: Mechanisms of action. J. Clin. Invest. 97, 2692–2696.

Rogers, M.J., Watts, D.J., Russell, R.G.G., 1997. Overview of bisphosphonates. Cancer 80, 1652–1660.

Rogers, M.J., Gordon, S., Beneford, H.L., Coxon, F.P., Luckman, S.P., Monkkonen, J., Frith, J.C., 2000. Cellular and molecular mechanisms of action of bisphosphonates. Cancer 88, 2961–2978.

Ruggiero, S.L., Mehrotra, B., Rosenberg, T.J., Engroff, S.L., 2004. Osteonecrosis of the jaws associated with the use of bisphosphonates: A review of 63 cases. J. Oral Maxillofac. Surg. 62, 527–534.

Ruggiero, S.L., Dodson, T.B., Assael, L.A., Landesberg, R., Marx, R.E., Mehrotra, B., American Association of Oral and Maxillofacial Surgeons, 2009. American Association of Oral and Maxillofacial Surgeons position paper on bisphosphonate-related osteonecrosis of the jaws — 2009 update. J. Oral Maxillofac. Surg. 67, 2–12.

Russell, R.G., Xia, Z., Dunford, J.E., Oppermann, U., Kwaasi, A., Hulley, P.A., Kavanagh, K.L., Triffitt, J.T., Lundy, M.Q., Phipps, R.J., Barnett, B.L., Coxon, F.P., Rogers, M.J., Watts, N.B., Ebetino, F.H., 2007. Bisphosphonates: An update on mechanisms of action and how else relate to clinical efficacy. Ann. N. Y. Acad. Sci. 1117, 209–257.

Sarasquete, M.E., Garcia-Sanz, R., Marin, L., Alcoceba, M., Chillon, M.C., Balanzategui, A., Santamaria, C., Rosinol, L., de la Rubia, J., Hernandez, M.T., Garcia-Navarro, I., Lahuerta, J.J., Gonzalez, M., San Miguel, J.F., 2008. Bisphosphonate-related osteonecrosis of the jaw is associated with polymorphisms of the cytochrome P450 CYP2C8 in multiple myeloma: A genome-wide single nucleotide polymorphism analysis. Blood 112, 2709–2712.

Schaudinn, C., Gorur, A., Webster, P., Jones, A.C., Neely, M., Jelliffe, R.W., Le, A.D., Sedghizadeh, P.P., 2012. Quantification by energy dispersive x-ray spectroscopy of alendronate in the diseased jaw bone of patients with bisphosphonate-related jaw osteonecrosis. Oral. Surg. Oral. Med. Oral. Pathol. Oral. Radiol. 114, 480–486.

Snover, J.L., Byrd, H., Suponeva, E.P., Vicenzi, E., Thompson, M.E., 1996. Growth and characterization of photoactive and electroactive zirconium bisphosphonate multilayer film. Chem. Mater. 8, 1490–1499.

Sugiyama, T., Uo, M., Wada, T., Hongo, T., Omagari, T., Komiyama, K., Sasaki, H., Takahashi, H., Kusama, M., Mori, Y., 2014. Novel metal allergy patch test using metal nanoballs. J. Nanobiotechnol. 12 (51), 1–6.

Sugiyama, T., Uo, M., Wada, T., Omagari, D., Komiyama, K., Noguchi, T., Jinbu, Y., Kusama, M., 2015. Estimation of trace metal element containing oral mucosa specimens by using SR-XRF, PIXE, and XAFS. BioMetals 28, 11–20.

Uo, M., Wada, T., Sugiyama, T., 2015. Applications of X-ray fluorescence analysis (XRF) to dental and medical specimens. Jpn. Dent. Sci. Rev. 51, 2–9.

Viereck, V., Emons, G., Lauck, V., Frosch, K.H., Blaschke, S., Gründker, C., Hofbauer, L.C., 2002. Bisphosphonates pamidronate and zoledronic acid stimulate osteoprotegerin production by primary human osteoblasts. Biochem. Biophys. Res. Commun. 291, 680–686.

Wessel, J.H., Dodson, T.B., Zavras, A.I., 2008. Zoledronate, smoking, and obesity are strong risk factors for osteonecrosis of the jaw: A case–control study. J. Oral Maxillofac. Surg. 66, 625–631.

Wolf, J.S., Stoller, M.L., 1994. Inhibition of calculi fragment growth by metal-bisphosphonate complexes demonstrated with a new assay measuring the surface activity of urolithiasis inhibitors. J. Urol. 152, 1609–1614.

Yoneda, T., Hagino, H., Sugimoto, T., Ohta, H., Takahashi, S., Soen, S., Taguchi, A., Toyosawa, S., Nagata, T., Urade, M., 2010. Bisphosphonate-related osteonecrosis of the jaw position paper from the allied Task Force Committee of Japanese Society for Bone and mineral Research, Japan Osteoporosis Society, Japanese Society of Periodontology, Japanese Society for oral and Maxillofacial Radiology, and Japanese Society of Oral and Maxillofacial Surgery. J. Bone Miner. Metab. 28, 365–383.